CHAPTER 3

TRI-MODE CONTROL AND SYNTHESIS OF THE EQUIVALENT ARMATURE CURRENT FOR REDUCING TORQUE RIPPLES

3.1 Introduction

As can be seen from chapter two, the linear relationship between the electromagnetic torque and the equivalent armature current of the PMBLDC motor renders the instantaneous torque control of the PMBLDC motor rather easy by simply regulating the equivalent armature current. Technically, there are many ways available to sense the equivalent armature current. However, in order to achieve a low cost drive, expensive sensors such as isolated galvanic current sensors should be avoid. Hence, in this chapter, a novel low cost current sensing technique which in fact can easily be integrated with the corresponding PWM inverter is proposed. Detailed sensing technique and its integration with the proposed tri-mode control strategy will be described in the following sections.

In section 3.2, a new sensing technique of the complete three phase currents of the PMBLDC is proposed. By using the proposed current sensing scheme, the proposed tri-mode control strategy for the PMBLDCM is then described in section 3.3. In section 3.4, synthesis of the equivalent armature current of PMBLDC motor is described and some simulation results are given in section 3.5 to demonstrate the effectiveness for reducing commutating torque ripples of the PMBLDC motor drive.

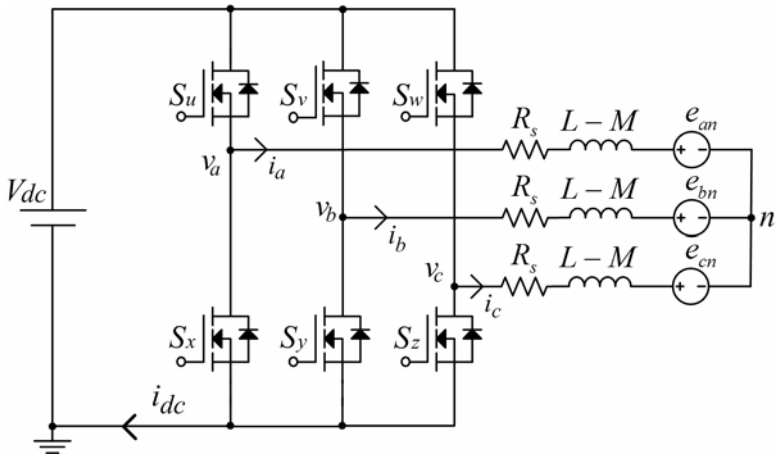

Fig. 3.1 Notations defined for the PMBLDC motor drive.

3.2 Sensing of the Complete Three-Phase Currents of PMBLDC Motors

For convenient explanation of the proposed sensing technique, typical notations are defined in Fig. 3.1. From Fig. 3.1 one can see that the three upper active switches are denoted as *Su, Sv,* and *Sw* while the lower ones are represented by *Sx, Sy,* and *Sz.* Also, the PMBLDC motor is represented with a decoupled three-phase load with neutral point n. Similarly, steady state ideal waveforms of the back emfs and the phase currents as well as the corresponding gating signals of the six active switches are shown in Fig. 3.2. For simplicity, six intervals are defined in Fig. 3.2 according to the ON or OFF states of the active switches. Thus, in the interval I where $t \in (\frac{\pi}{3\omega_e}, \frac{2\pi}{3\omega_e})$ one can see from Fig. 3.2 that switches *Su* and *Sy* are ON. Similarly, for the remaining five intervals, only two switches are ON where one switch is in the upper arm of the inverter and the other is located in the lower arm. In other words, during each interval, from the viewpoint of the PMBLDC motor, only two phases are connected to the dc voltage source through the inverter switches.

However, in practical dynamic situation, proper PWM control of the inverter is required to keep the phase current constant. Depending on the PMBLDC motor driving

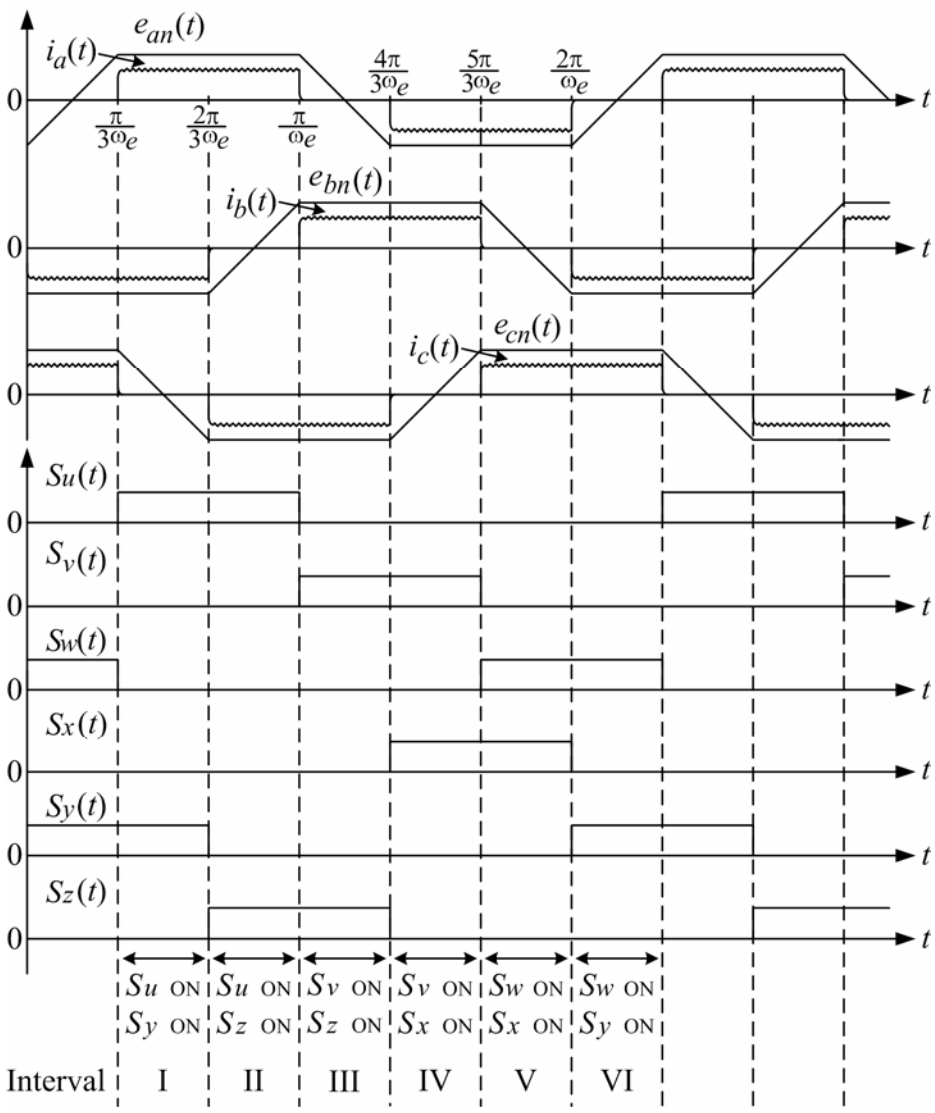

Fig. 3.2 Steady state ideal waveforms of the back emfs, phase currents and the corresponding gating signals.

condition, there are three control modes, namely active mode, freewheeling mode and the regenerative mode. First consider the case that the PMBLDC motor is under driving condition, then the active and freewheeling modes are alternatively applied to achieve the desired equivalent dc current. As an illustrative example, supposed that in interval I, then the three control modes are shown in Fig. 3.3. From Fig. 3.3(a) it is seen that for this active mode, the resulting current i_{dc} will increase due to the applied V_{dc}. In other words, energy is supplied to the motor as well as stored in the inductors of the stator windings of phases a and b. Also, from Fig. 3.3(b) one can see that for this freewheeling mode, *Su* is turned off and the resulting circulating current will decrease due to energy loss of the winding resistances and the switch ON resistances. Hence, under driving condition, by simply switching ON and OFF of *Su* while keeping *Sy* ON, one can increase or keep i_{dc} to the desired value. Meanwhile from Figs. 3.3(a) and 3.3(b) it is quite obvious that current i_a or i_b in fact is equal to the current through *Sy*. Next, consider the braking condition of the PMBLDC motor. Under this braking condition, one can see from (2.22) that in order to reduce the torque it is required to reduce i_{eq}. Thus, switch *Su* is turned OFF to cut off the dc power supply. Due to continuity of the phase current, it is seen from Fig. 3.3(c) that the resulting current will flow to the dc source through the body diodes of *Sx* and *Sv*. In other words, unlike the previous driving case, now a reverse dc voltage, namely $-V_{dc}$, is applied to the PMBLDC motor such that i_{dc} is reduced. In order to control i_{eq} to a smaller value, the freewheeling mode in Fig. 3.3(b) is also required. Thus, by switching *Sy* ON and OFF alternatively while keeping *Su* in OFF state, one can control i_{eq} to the desired value. Meanwhile, by observing Figs. 3.3(b) and 3.3(c) one can see that during this braking condition and in this interval, phase currents i_a and i_b are in fact equal to the current through *Sx* switch.

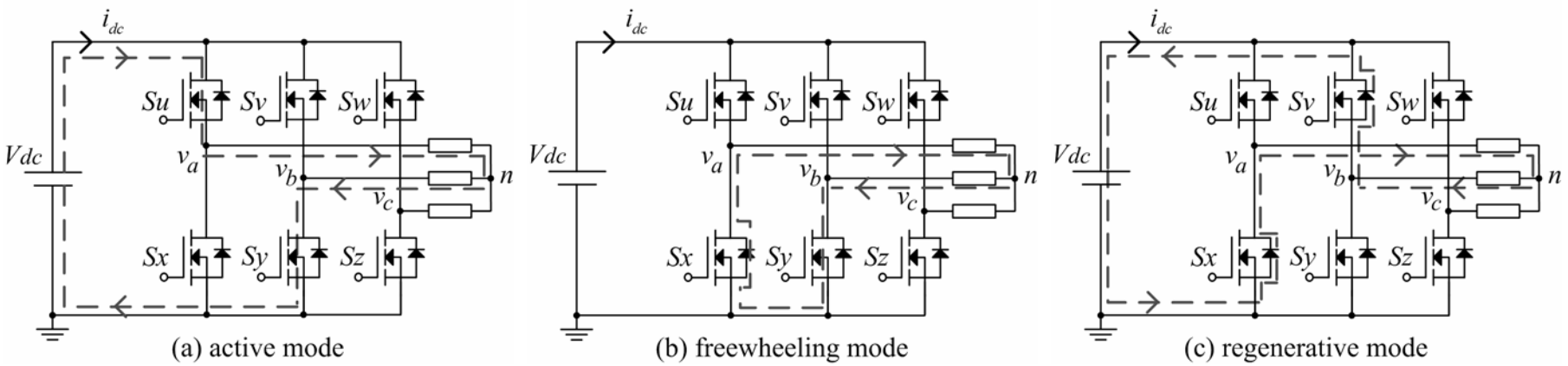

Fig. 3.3 Current flow diagrams under three control modes for interval I. (a) active mode. (b) freewheeling mode. (c) regenerative mode.

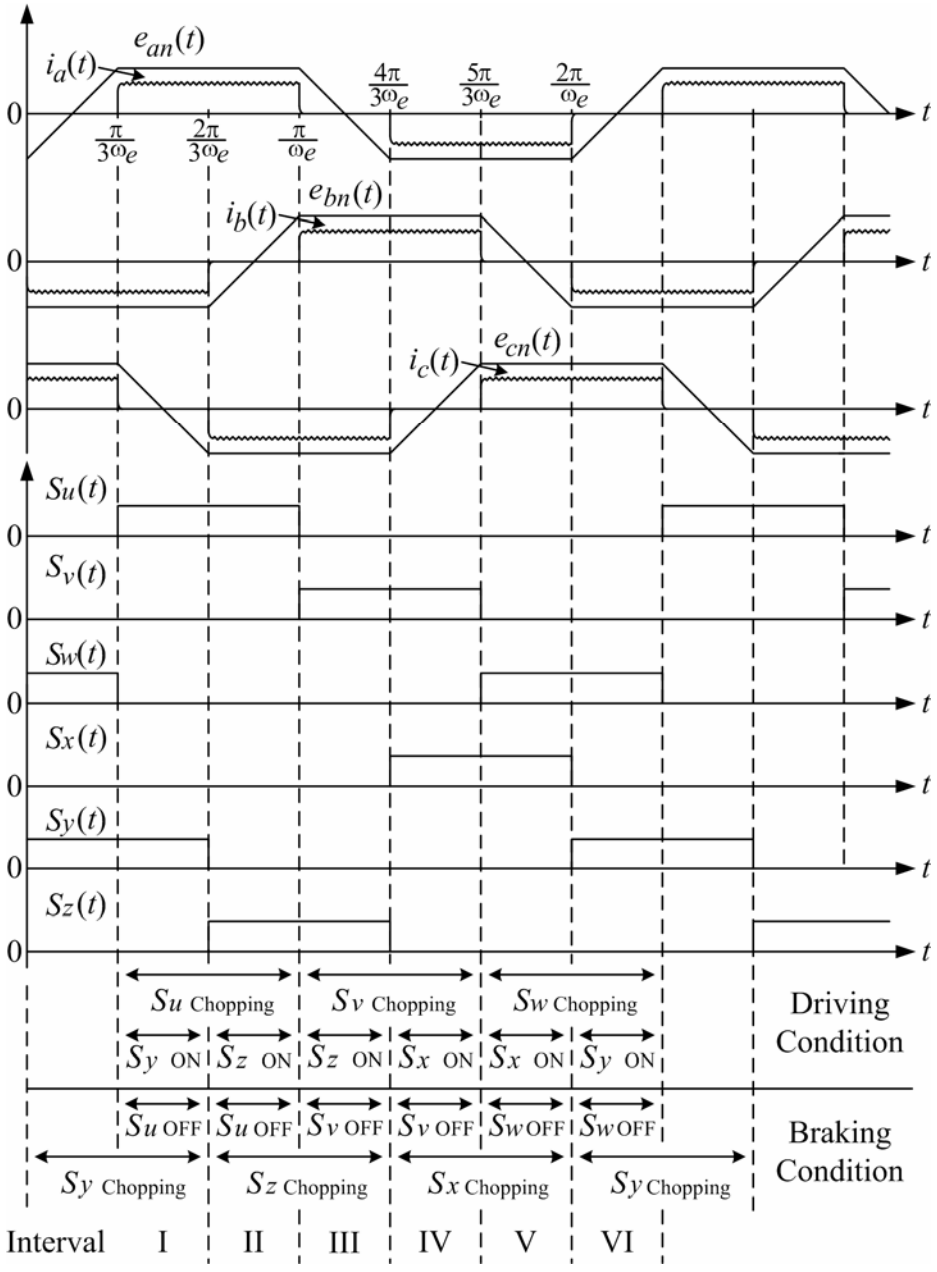

Fig. 3.4 Schematic diagram of the PWM control under driving and braking conditions.

Similarly, one can obtain the results for the other intervals as shown in Fig. 3.4. It is seen from Fig. 3.4 that under driving condition the PWM control involves both active mode and freewheeling mode while under braking condition only regenerative and freewheeling modes are involved. Once the current flow paths of the PMBLDC motor under dynamic control for the six intervals are known, it is now very easy to understand how the proposed sensing scheme can be used to measure the phase currents. Again, for simplicity, only the first time interval will be explained. Fig. 3.5 shows the sensing scheme for three control modes within the first interval. From Fig. 3.5 one can see that three current shunts, namely *Rx*, *Ry* and *Rz* are connected in series with *Sx*, *Sy* and *Sz* respectively and with the same ground. Therefore from Figs. 3.5(a) and 3.5(b) one can see that under driving condition and within interval I, $i_a = -i_b = i_{Ry}$. Similarly, from Figs. 3.5(b) and 3.5(c) it is seen that under braking condition and within interval I, $i_a = -i_b = -i_{Rx}$. Table 3.1 summarizes the proposed phase current sensing scheme for a complete cycle. From Table 3.1 one can see that, using interval I as an example, if under driving condition, one can measure i_{Ry} to get the complete phase currents, namely $i_a = i_{Ry}$, $i_b = -i_{Ry}$ and $i_c = 0$. Similarly, if under braking condition, then one can measure i_{Rx} to get all phase currents, namely, $i_a = -i_{Rx}$, $i_b = i_{Rx}$ and $i_c = 0$. Thus, the remaining problem lies in how to synthesize all phase currents to get i_{eq} efficiently. However, before synthesizing i_{eq} it is necessary to understand the proposed tri-mode control in advance.

3.3 The Proposed Tri-Mode Control of the Equivalent Armature Current

As discussed in the first chapter, to reduce torque ripples, except under transient condition, excessive energy input to the PMBLDC motor should be avoided. For example, the two-mode control strategy uses only active and regenerative modes [38]. As a result,

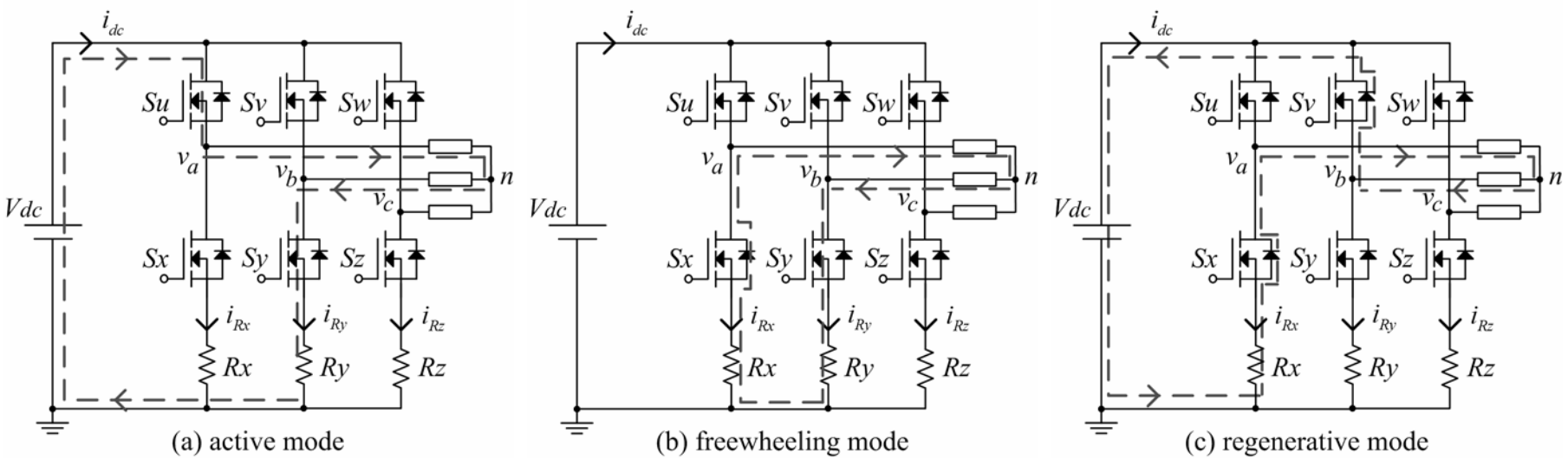

Fig. 3.5 The proposed current sensing scheme under three control modes for interval I. (a) active mode. (b) freewheeling mode. (c) regenerative mode.

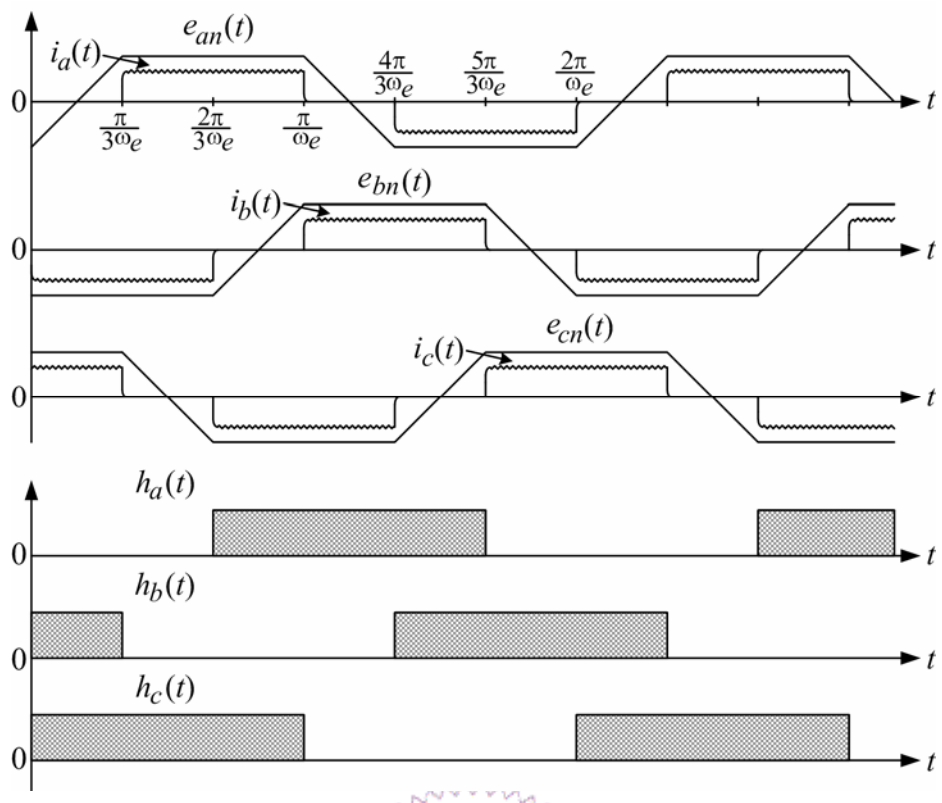

Fig. 3.6 Hall sensor signals of the PMBLDC motor.

the regenerative mode control will always exist even under steady state. On the other hand, by using the proposed tri-mode control the power flow direction will always be from the dc voltage source to the PMBLDC motor under steady state. More specifically, under driving condition such as during starting or acceleration, only the active mode and the freewheeling mode are alternatively used to control the equivalent armature current, i_{eq}, to the desired value. Similarly, under braking condition such as during braking or deceleration, only the regenerative mode and the freewheeling mode are alternatively used to control the equivalent armature current to the desired value. Mathematically, one can define binary variable C_{sign} as follow:

$$C_{sign} = \begin{cases} 0, & \text{if } i_s - i_{eq} \geq 0 \\ 1, & \text{if } i_s - i_{eq} < 0 \end{cases} \tag{3.1}$$

where i_s is the command signal of i_{eq}. It follows from (3.1) that if $C_{sign} = 0$ then the PMBLDC is under driving condition while if $C_{sign} = 1$ then the motor is under braking condition.

Next, consider the locating of the six intervals. Fig. 3.6 shows the typical waveforms of the three Hall sensor signals as well as the corresponding back emf waveforms. It is seen from Fig. 3.6 that the Hall sensor signals, namely $h_a(t)$, $h_b(t)$ and $h_c(t)$, have a phase delay of $\frac{\pi}{3}$ from the respective phase currents, namely $i_a(t)$, $i_b(t)$ and $i_c(t)$. Also, from Figs. 2.4 and 3.6 one can observe the relationship among $e_{an}(t)$, $i_a(t)$, $Sa(t)$ and the gating signal $Su(t)$ in Fig. 3.2. It turns out that now one can use $h_a(t)$, $h_b(t)$ and $h_c(t)$ to code the six intervals as shown in Table 3.2 where for convenient reference, the corresponding switching states under steady state, namely *u, v, w, x, y, z* according to Fig. 3.2 are also listed.

Once the time interval is located and in case C_{sign} is known, then the remaining task is to determine the duty ratio of the active (regenerative) mode in case C_{sign} is 0 (1). Fig. 3.7 shows how the corresponding duty ratio is generated. From Fig. 3.7 one can see that a constant clock signal, CK, is input to the counter and then to digital-to-analog converter to generate a triangular waveform. The control signal, namely $i_s - i_{eq}$, after a PI controller is then compared with the triangular wave to generate the V_{PWM} signal. From the previous tri-mode control principle, it is seen that within a clock signal period the active (regenerative) mode time period of the PWM control, namely when $V_{PWM} = 1$, can be determined when the controller is in driving (braking) mode. The remaining time period,

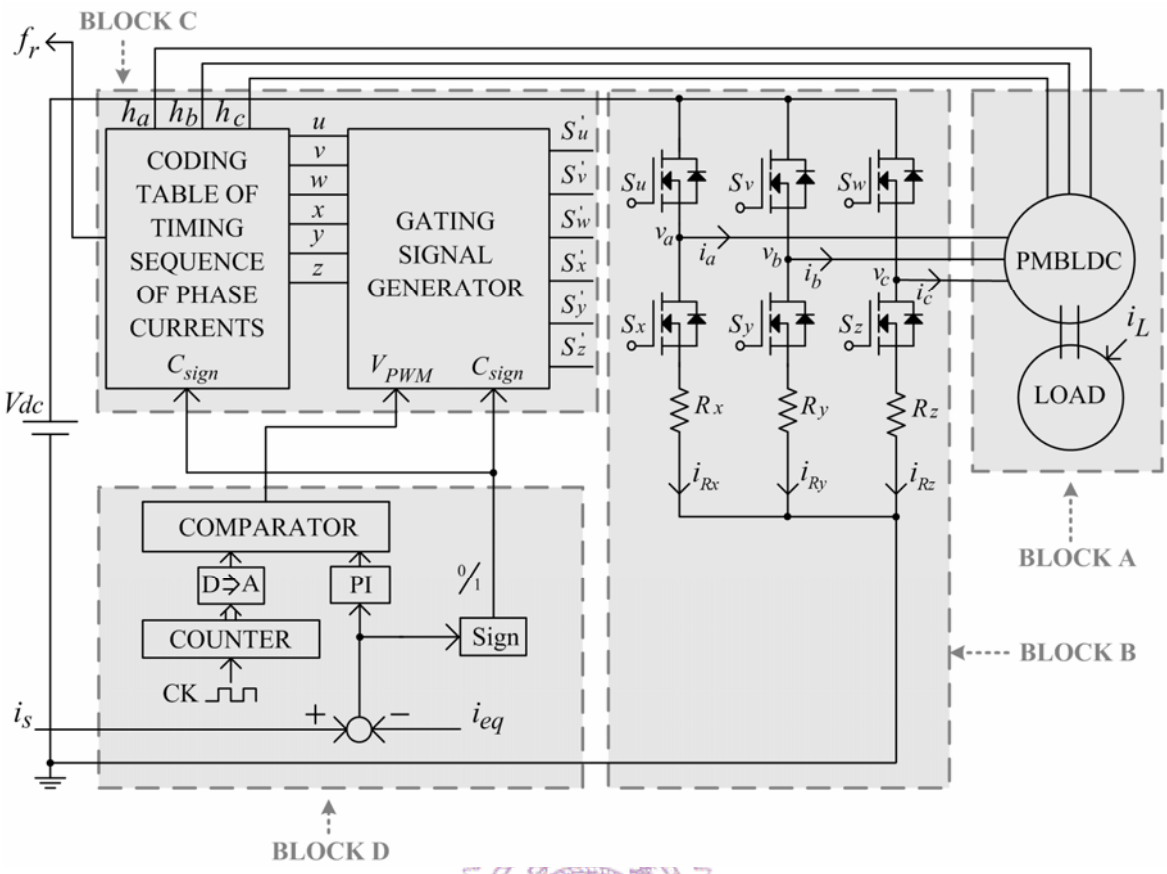

Fig. 3.7 The block diagram of the integrated phase current sensing and equivalent armature current control system.

namely when $V_{PWM} = 0$, is in fact under freewheeling control mode. It follows that the desired gating signal, namely *Su', Sv', Sw', Sx', Sy'* and *Sz'*, can be determined as shown in Table 3.3. From Table 3.3 one can see that for easy understanding, in each interval, an additional alphabet (A, F, R) is attached to denote one of the three control modes, namely Active mode, Freewheeling mode and the Regenerative mode. Also, for convenient references, the steady state switch status, (*u, v, w, x, y, z*) are also listed. It is seen that the actual dynamic control signals (*Su', Sv', Sw', Sx', Sy', Sz'*) are closely related to the steady

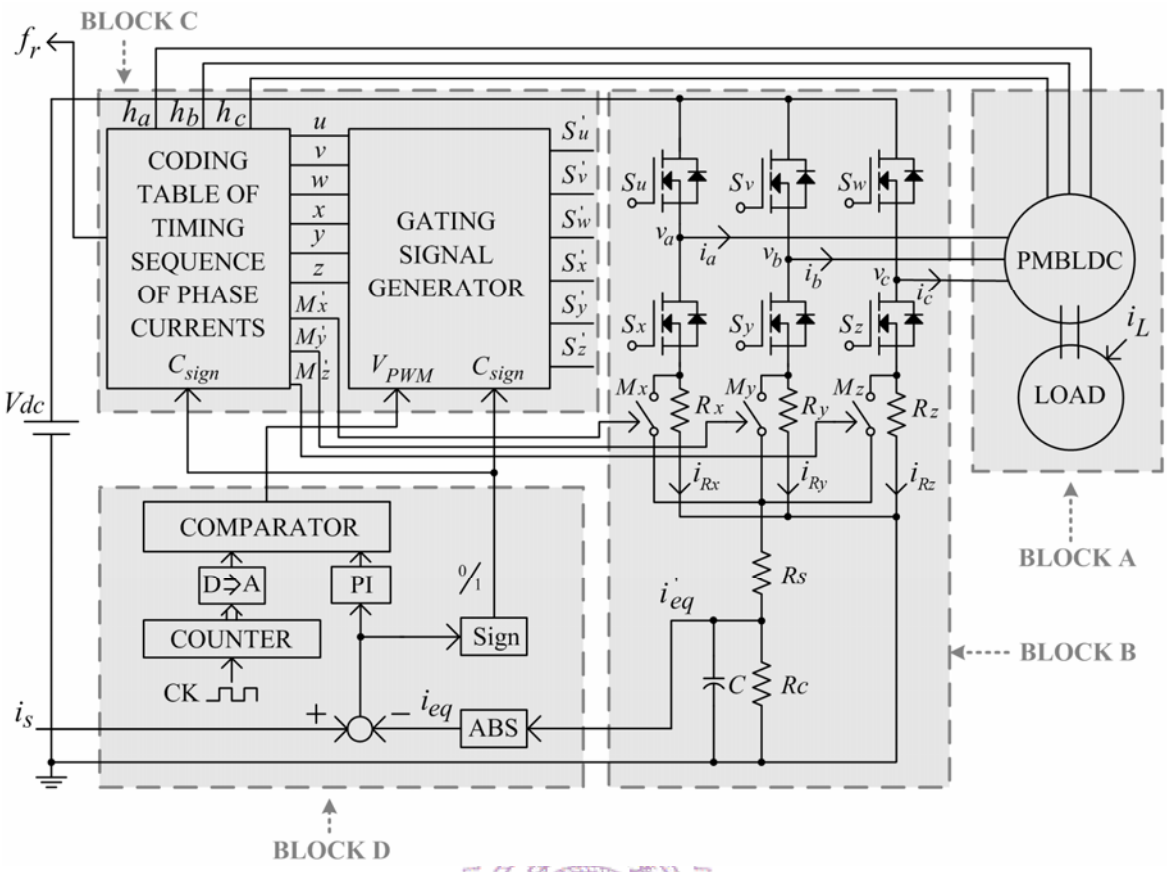

Fig. 3.8 The block diagram of the integrated phase current sensing and equivalent armature current synthesize and control system.

state switch status. In other words, under driving condition, one of the upper switches is switched ON and OFF such that the active mode and the freewheeling mode are alternatively operated while under braking condition, one of the lower switches is switched ON and OFF such that the regenerative mode and the freewheeling mode are alternatively operated as can be observed from Fig. 3.3.

Table 3.1 The Proposed Phase Current Sensing Scheme.

Interval	I		II		III		IV		V		VI	
D & B / Current	D	B	D	B	D	B	D	B	D	B	D	B
i_a	(○) i_{Ry}	(○) $-i_{Rx}$	(○) i_{Rz}	(○) $-i_{Rx}$	0	0	$-i_{Rx}$	i_{Ry}	$-i_{Rx}$	i_{Rz}	0	0
i_b	$-i_{Ry}$	i_{Rx}	0	0	(○) i_{Rz}	(○) $-i_{Ry}$	(○) i_{Rx}	(○) $-i_{Ry}$	0	0	$-i_{Ry}$	i_{Rz}
i_c	0	0	$-i_{Rz}$	i_{Rx}	$-i_{Rz}$	i_{Ry}	0	0	(○) i_{Rx}	(○) $-i_{Rz}$	(○) i_{Ry}	(○) $-i_{Rz}$

D : representing driving condition

B : representing braking condition

○ : representing the selected sensing current

Table 3.2 Interval Locating from h_a, h_b, h_c and the Corresponding Steady-State Switch Status.

Interval	h_a	h_b	h_c	u	v	w	x	y	z
I	0	0	1	1	0	0	0	1	0
II	1	0	1	1	0	0	0	0	1
III	1	0	0	0	1	0	0	0	1
IV	1	1	0	0	1	0	1	0	0
V	0	1	0	0	0	1	1	0	0
VI	0	1	1	0	0	1	0	1	0

Table 3.3 Coding Table of the Gating Signal Generator

Interval	C_{sign}	V_{PWM}	u	v	w	x	y	z	Su'	Sv'	Sw'	Sx'	Sy'	Sz'
I-A	0	1	1	0	0	0	1	0	1	0	0	0	1	0
I-F	×	0	1	0	0	0	1	0	0	0	0	0	1	0
I-R	1	1	1	0	0	0	1	0	0	0	0	0	0	0
II-A	0	1	1	0	0	0	0	1	1	0	0	0	0	1
II-F	×	0	1	0	0	0	0	1	0	0	0	0	0	1
II-R	1	1	1	0	0	0	0	1	0	0	0	0	0	0
III-A	0	1	0	1	0	0	0	1	0	1	0	0	0	1
III-F	×	0	0	1	0	0	0	1	0	0	0	0	0	1
III-R	1	1	0	1	0	0	0	1	0	0	0	0	0	0
IV-A	0	1	0	1	0	1	0	0	0	1	0	1	0	0
IV-F	×	0	0	1	0	1	0	0	0	0	0	1	0	0
IV-R	1	1	0	1	0	1	0	0	0	0	0	0	0	0
V-A	0	1	0	0	1	1	0	0	0	0	1	1	0	0
V-F	×	0	0	0	1	1	0	0	0	0	0	1	0	0
V-R	1	1	0	0	1	1	0	0	0	0	0	0	0	0
VI-A	0	1	0	0	1	0	1	0	0	0	1	0	1	0
VI-F	×	0	0	0	1	0	1	0	0	0	0	0	1	0
VI-R	1	1	0	0	1	0	1	0	0	0	0	0	0	0

A : representing active mode

F : representing freewheeling mode

R : representing regenerative mode

Table 3.4 Coding Table of the Gating Signals *Mx'*, *My'* and *Mz'*

Interval	C_{sign}	h_a	h_b	h_c	u	v	w	x	y	z	Mx'	My'	Mz'
I-D	0	0	0	1	1	0	0	0	1	0	0	1	0
I-B	1	0	0	1	1	0	0	0	1	0	1	0	0
II-D	0	1	0	1	1	0	0	0	0	1	0	0	1
II-B	1	1	0	1	1	0	0	0	0	1	1	0	0
III-D	0	1	0	0	0	1	0	0	0	1	0	0	1
III-B	1	1	0	0	0	1	0	0	0	1	0	1	0
IV-D	0	1	1	0	0	1	0	1	0	0	1	0	0
IV-B	1	1	1	0	0	1	0	1	0	0	0	1	0
V-D	0	0	1	0	0	0	1	1	0	0	1	0	0
V-B	1	0	1	0	0	0	1	1	0	0	0	0	1
VI-D	0	0	1	1	0	0	1	0	1	0	0	1	0
VI-B	1	0	1	1	0	0	1	0	1	0	0	0	1

D : representing driving condition

B : representing braking condition

3.4 Synthesis of the Equivalent Armature Current of PMBLDC Motors

Once the above tri-mode control is understood, the actual switching status can be determined easily. Hence, the remaining task is to synthesis the desired i_{eq} by using the previous current shunts, namely *Rx, Ry* and *Rz*. Hence, three low cost transmission gates *Mx, My* and *Mz* are added with a common node as shown in Fig. 3.8 where a voltage divider with *Rs* and *Rc* is used to extract the current signal. Also, in order to reduce the noise a capacitor, C, is paralleled with *Rc* to filter the high frequency noise. In addition,

from Table 3.1 one can see that under braking condition the direction of the current through the shunt (*Rx, Ry, Rz*) is in fact reversed. Therefore, the output signal $i_{eq}^{'}$ of the *RcC* low pass filter is processed by an absolute value device to synthesize the desired i_{eq}. It should be mentioned here that due to choosing an industrial blower as the application carrier in this dissertation, only the motor mode with two quadrant operation is considered. Hence, a simple absolute value device is adopted. Now, consider the control of the *Mx, My,* and *Mz* transmission gates such that desired i_{eq} can be synthesized. It is seen from Tables 3.1 and 3.2 that gating signals namely *Mx', My'* and *Mz'* can be obtained as shown in Table 3.4. From Table 3.4 one can see that for convenient reference, the corresponding steady state switch status (*u, v, w, x, y, z*) is also listed. For easy reference, each interval is distinguished further into under Driving condition or under Braking condition according to C_{sign} as shown in Table 3.4.

Finally, to have a better overall view about the proposed tri-mode control, Fig. 3.9 to 3.14 shows the complete operation modes for different intervals. The detailed principle has been described previously and will not be repeated here.

3.5 Simulation Results of the Proposed Tri-Mode Equivalent Armature Current Controlled PMBLDC Motor System

In order to show the validity and effectiveness of the proposed Tri-Mode control of the equivalent armature current for the PMBLDC motor, the following simulations are made. Suppose the PMBLDC motor with phase resistance $R_s = 3\Omega$, phase inductance $L - M = 7\text{mH}$ and with perfect peak trapezoidal back emfs $\pm 50\text{V}$ and is controlled by the proposed current controller as shown in Fig. 3.8. The simulation results of the motor phase

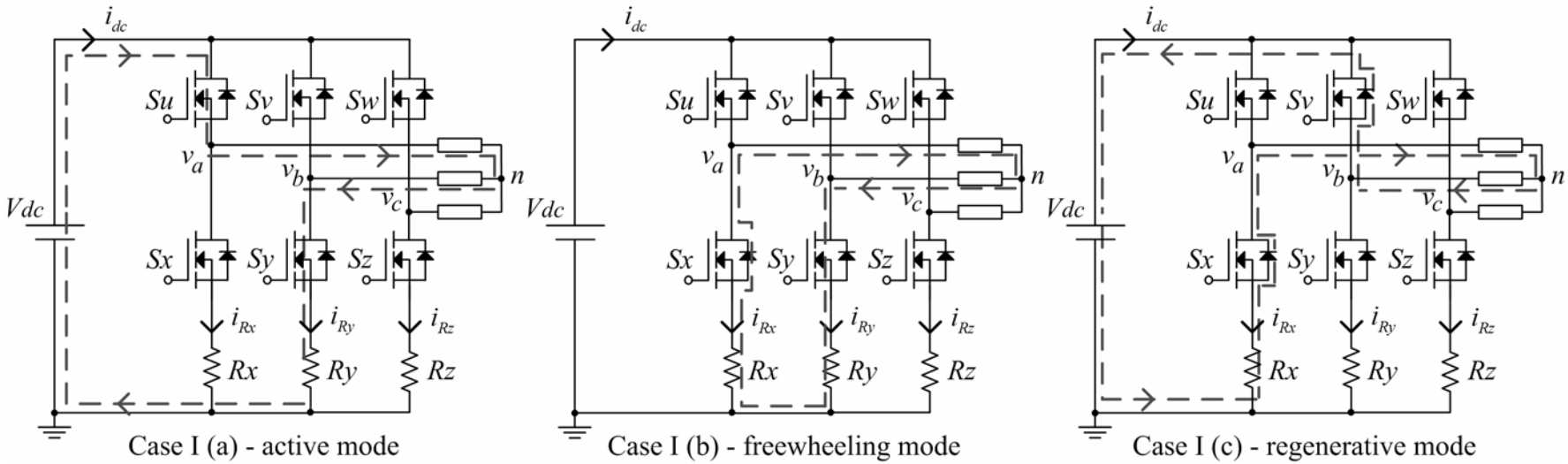

Fig 3.9 Complete operation modes for the proposed equivalent armature current sensing and synthesis method cases I(a), I(b) and I(c) in interval I.

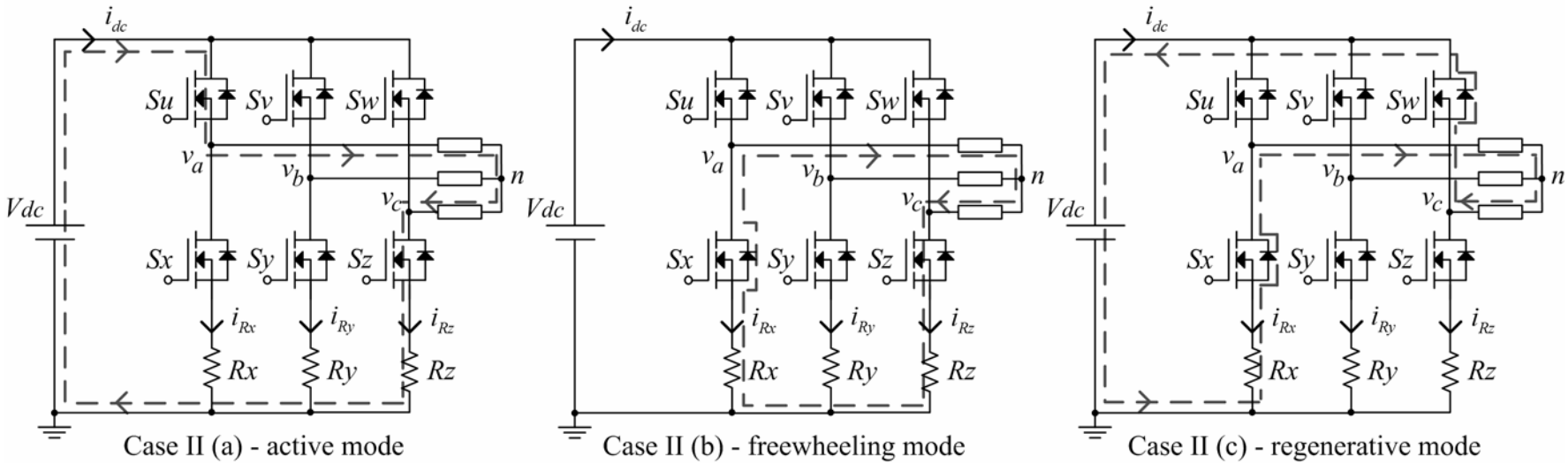

Fig 3.10 Complete operation modes for the proposed equivalent armature current sensing and synthesis method cases II(a), II(b) and II(c) in interval II.

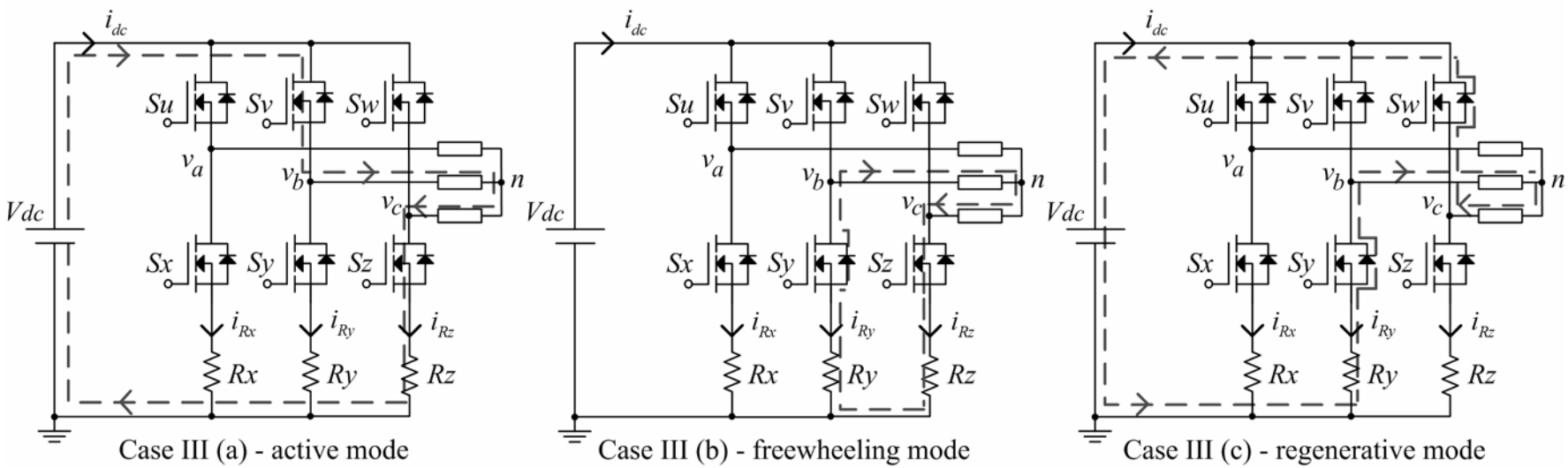

Fig 3.11 Complete operation modes for the proposed equivalent armature current sensing and synthesis method cases III(a), III(b) and III(c) in interval III.

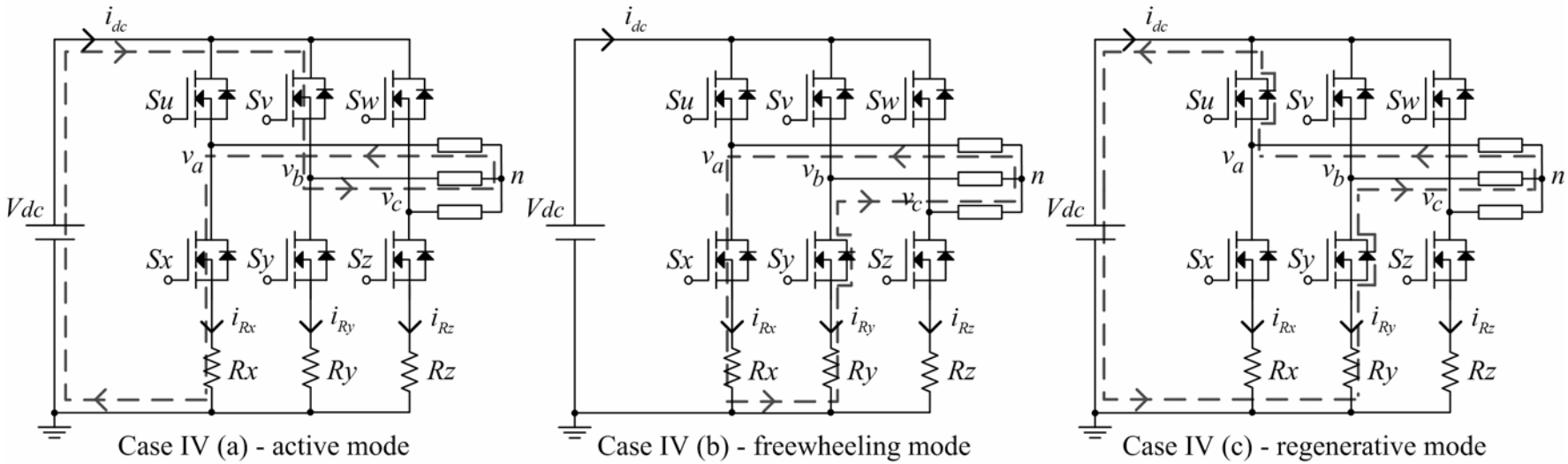

Fig 3.12 Complete operation modes for the proposed equivalent armature current sensing and synthesis method cases IV(a), IV(b) and IV(c) in interval IV.

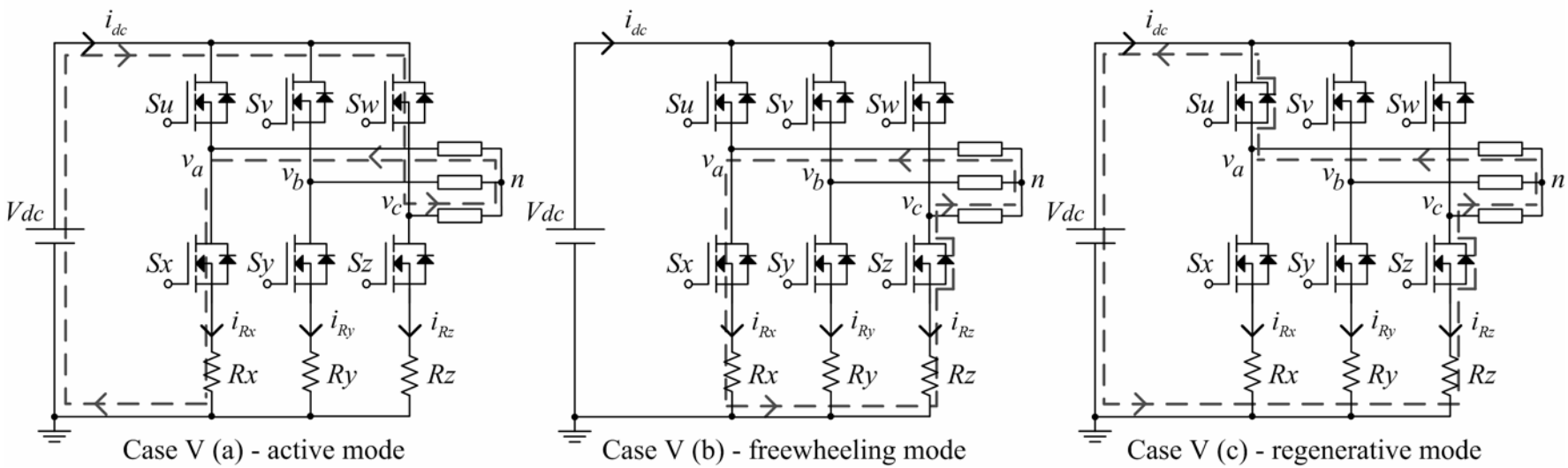

Fig 3.13 Complete operation modes for the proposed equivalent armature current sensing and synthesis method cases V(a), V(b) and V(c) in interval V.

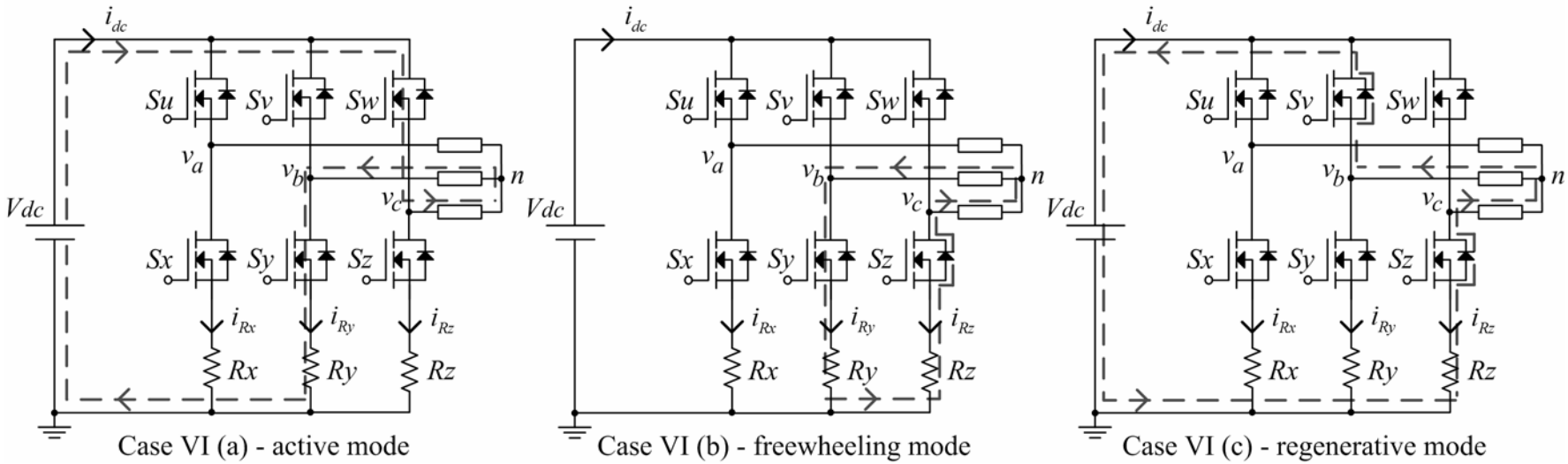

Fig 3.14 Complete operation modes for the proposed equivalent armature current sensing and synthesis method cases VI(a), VI(b) and VI(c) in interval VI.

currents, the equivalent armature current and the electromagnetic torque with equivalent armature current regulation of the proposed current controller are shown in Fig. 3.15, while the simulation time period covers intervals I and II. As shown in Fig. 3.15, initially the conduction phases of the PMBLDC motor are phase a and b, then b-phase current is switched c-phase. Therefore, during this time interval, the equivalent armature current is initially equal to a-phase current or negative b-phase current. After commutation, the equivalent armature current will be equal to a-phase current or negative c-phase current. From Fig.3.15(a) one can see that the equivalent armature current of the PMBLDC motor is regulated very well in spite of the phase current commutation. It also can be observed that the generating torque of the PMBLDC motor is proportional to the controlled equivalent armature current and remains almost constant during the phase current commutation. The detailed waveform under commutation process is amplified as shown in Fig. 3.15(b). From Fig. 3.15(b) one can see that since the equivalent armature current as well as the a-phase current are controlled to be nearly constant, the slope magnitude of the incoming c-phase current and the slope magnitude of the outgoing b-phase current will be almost equalized. Hence the commutation electromagnetic torque ripples are suppressed automatically [38]. For comparison, the same case is simulated without i_{eq} control and the result is shown in Fig. 3.16. From Fig. 3.16, one can see that the commutating torque ripple is rather significant. Practically, the back emf waveform is not so perfect as assumed in the previous ideal condition. To be more close to the practical situation, assume the back emf waveform obtained from approximating a practical PMBLDC motor as shown in Fig. 3.17 is adopted for simulation. All other simulation conditions are kept unchanged. The simulation results without and with the proposed i_{eq} control are shown in Figs. 18 and 19 respectively. It is found that although the closed loop i_{eq} control result is much better than

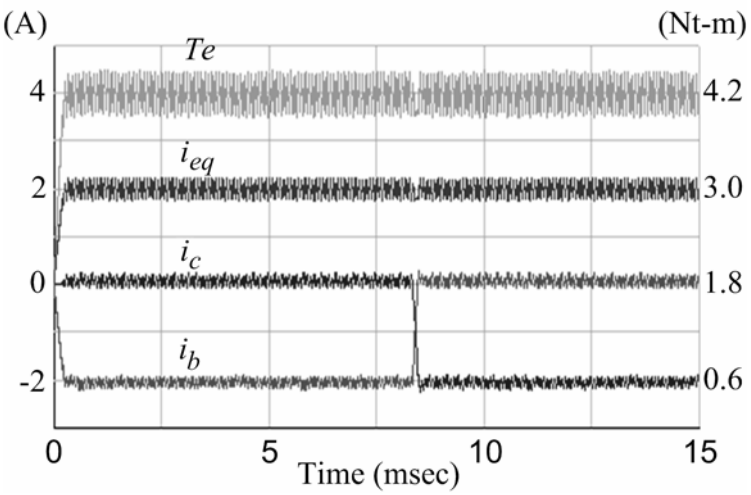

(a)

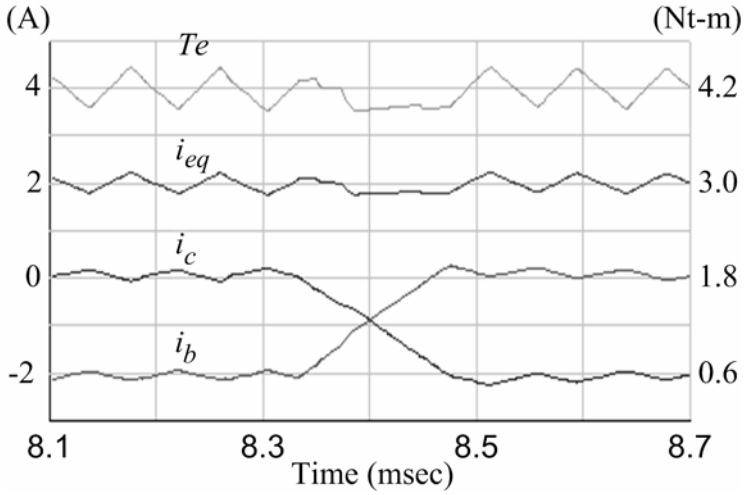

(b)

Fig. 3.15 Transient simulation results of i_b, i_c, i_{eq} and T_e with the proposed equivalent armature current control under commutation process assuming ideal trapezoidal back emfs.

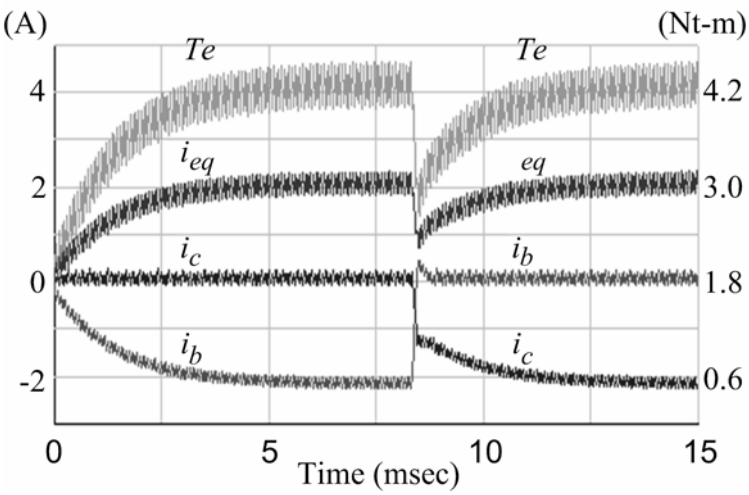

Fig. 3.16 Transient simulation results of i_b, i_c, i_{eq} and T_e without the proposed equivalent armature current control under commutation process assuming ideal trapezoidal back emfs.

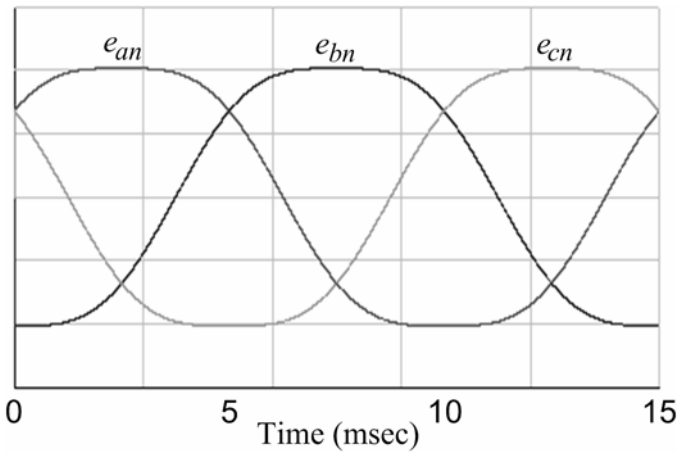

Fig. 3.17 Trapezoidal back emfs with spreading angle around 100°.

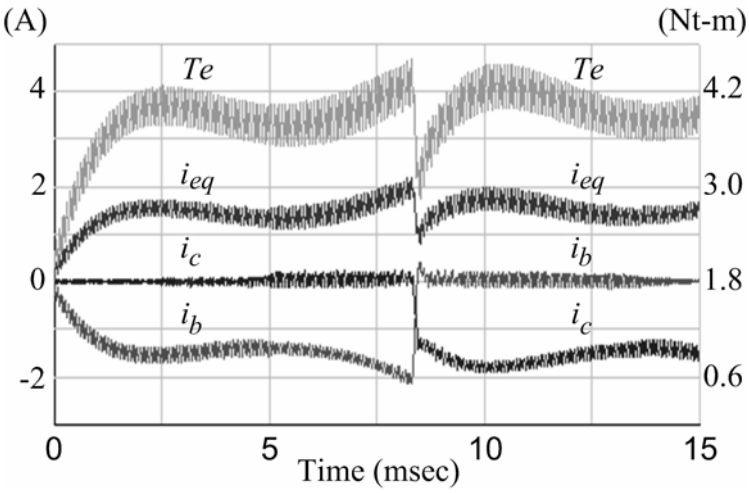

Fig. 3.18 Transient simulation results of i_b, i_c, i_{eq} and T_e without the proposed equivalent armature current control under commutation process assuming non-ideal trapezoidal back emfs.

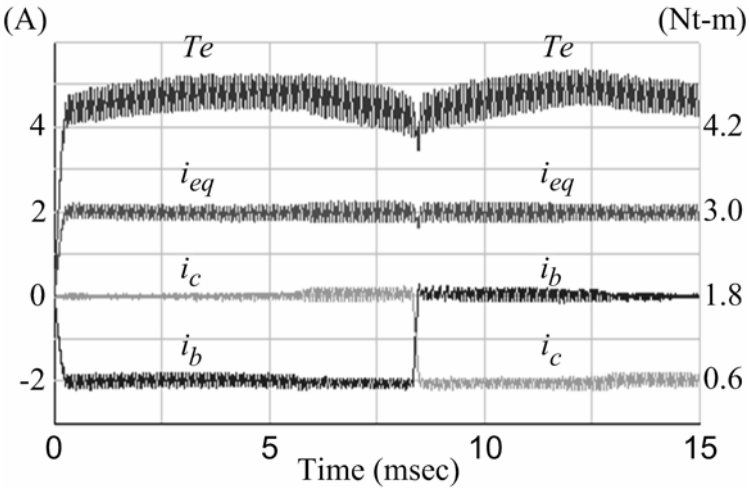

Fig. 3.19 Transient simulation results of i_b, i_c, i_{eq} and T_e with the proposed equivalent armature current control under commutation process assuming non-ideal trapezoidal back emfs.

without i_{eq} control, however, due to the non-ideal back emf, the resulting torque is also degraded.

From the simulation results shown in the above Figs., one can summarize that due to the effectiveness of the proposed Tri-Mode control, the equivalent armature current of the PMBLDC motor can be controlled instantaneously. As a result, not only the electromagnetic torque of the PMBLDC motor can have nice dynamic response, but also the pulsating torque ripple can be reduced automatically and greatly.